LBL-30395
Preprint

Lawrence Berkeley Laboratory
UNIVERSITY OF CALIFORNIA

Submitted to Annals of Physics

A Thomas-Fermi Model of Nuclei
Part II: Fission Barriers and Charge Distributions

W.D. Myers and W.J. Swiatecki

March 1991

U. C. Lawrence Berkeley Laboratory
Library, Berkeley

FOR REFERENCE

Not to be taken from this room

LBL-30395
Copy 1
Bldg. 50 Library.

Prepared for the U.S. Department of Energy under Contract Number DE-AC03-76SF00098

DISCLAIMER

This document was prepared as an account of work sponsored by the United States Government. Neither the United States Government nor any agency thereof, nor The Regents of the University of California, nor any of their employees, makes any warranty, express or implied, or assumes any legal liability or responsibility for the accuracy, completeness, or usefulness of any information, apparatus, product, or process disclosed, or represents that its use would not infringe privately owned rights. Reference herein to any specific commercial products process, or service by its trade name, trademark, manufacturer, or otherwise, does not necessarily constitute or imply its endorsement, recommendation, or favoring by the United States Government or any agency thereof, or The Regents of the University of California. The views and opinions of authors expressed herein do not necessarily state or reflect those of the United States Government or any agency thereof or The Regents of the University of California and shall not be used for advertising or product endorsement purposes.

Lawrence Berkeley Laboratory is an equal opportunity employer.

DISCLAIMER

This document was prepared as an account of work sponsored by the United States Government. While this document is believed to contain correct information, neither the United States Government nor any agency thereof, nor the Regents of the University of California, nor any of their employees, makes any warranty, express or implied, or assumes any legal responsibility for the accuracy, completeness, or usefulness of any information, apparatus, product, or process disclosed, or represents that its use would not infringe privately owned rights. Reference herein to any specific commercial product, process, or service by its trade name, trademark, manufacturer, or otherwise, does not necessarily constitute or imply its endorsement, recommendation, or favoring by the United States Government or any agency thereof, or the Regents of the University of California. The views and opinions of authors expressed herein do not necessarily state or reflect those of the United States Government or any agency thereof or the Regents of the University of California.

LBL - 30395

A Thomas-Fermi Model of Nuclei Part II: Fission Barriers and Charge Distributions *

W.D. Myers and W.J. Swiatecki

Nuclear Science Division

Lawrence Berkeley Laboratory

1 Cyclotron Road

Berkeley, California 94720

*This work was supported by the Director, Office of Energy Research, Office of High Energy and Nuclear Physics, Nuclear Physics Division of the US Department of Energy under Contract DE - AC03 - 76SF00098.

Abstract

The Thomas-Fermi model of average nuclear properties described in Part I [1] is simplified further and then applied to the calculation of fission barriers and charge distributions. An extensive comparison with experimental data reveals a small but clear-cut barriers vs. size discrepancy: if the radius constant r_0 is chosen to be 1.13 fm so as to reproduce measured nuclear sizes, the calculated fission barriers are too high. The suggestion is made that an extension of the Thomas-Fermi method is called for in order to describe the presence in nuclei of the "quantal halo," i.e. of the classically forbidden region around the nuclear surface where matter exists at negative kinetic energy.

Contents

1 Introduction 4

2 The Simplified Thomas-Fermi Model 6

2.1 The effective nucleon-nucleon interaction 6

2.2 The simplified Thomas-Fermi energy 8

2.3 Uniform nuclear matter 11

2.4 The nuclear potential inside a finite nucleus 11

2.5 The Euler equations 13

2.6 Estimating the adjustable parameters 14

3 Fission Barriers 20

4 Charge Distributions 29

5 Discussion 33

6 Appendix A 35

7 Appendix B 37

8 Acknowledgements 45

1 Introduction

In Part I [1] a model of average nuclear properties was formulated. It was based on a statistical treatment of the nuclear energy, analogous to the Thomas-Fermi approximation for the description of smoothed electron densities in atoms and molecules. In place of the electrostatic interactions between atomic electrons, an effective short-range nucleon-nucleon potential was introduced, representing a generalization of the momentum-dependent Seyler-Blanchard Yukawa interaction. The resulting model was used to discuss nuclear binding energies, sizes and charge distributions, as well as the relation of the nuclear compressibility to the surface energy and surface diffuseness. The nuclear optical model potential, including its energy and isospin dependences was also calculated. In Part I [1] the model was applied to nuclei assumed to be spherically symmetric. In the present paper we generalize the discussion to arbitrary nuclear shapes, which makes possible the crucial confrontation of the model with measurements of nuclear fission barriers. (An extensive program of studies along similar lines is described in [2] or [3–5].)

In the course of these developments a certain modification of the effective nucleon-nucleon interaction was introduced, which further simplifies the algebraic structure of the model. The simplification consists in shortening the range in the saturating part of the nucleon-nucleon interaction all the way to the limiting case of a zero-range delta function. We begin by summarizing, in Section 2, the equations defining this simplified model. This summary is

meant to be self-contained, but the reader is encouraged to consult Part I for the background discussions. Section 3 presents the results of applying the model to the calculation of fission barriers and Section 4 compares calculated and measured charge distributions for a sample of spherical nuclei. Section 5 focuses on the resulting barriers vs. size discrepancy and suggests a possible resolution.

2 The Simplified Thomas-Fermi Model

2.1 The effective nucleon-nucleon interaction

Using the Fermi energy of standard nuclear matter, T_0, as unit of energy, and using $\hat{\rho}$, equal to half the density ρ_0 of standard nuclear matter, as unit of density, we write the interaction potential $v(r_{12})$ between two nucleons at a separation r_{12} in the following form:

$$v(r_{12}) = v_{\text{direct}} + v_{\text{saturating}} \,, \tag{1}$$

where,

$$\begin{aligned} \frac{v_{\text{dir}}(r_{12})}{T_0} &= -\frac{1}{2}(1 \mp \xi)\alpha\hat{\rho}^{-1} f\left(\frac{r_{12}}{a}\right) \,, \\ \frac{v_{\text{sat}}(r_{12})}{T_0} &= \frac{1}{2}(1 \mp \zeta)\left[\beta\left(\frac{p_{12}}{P_0}\right)^2 - \gamma\left(\frac{p_{12}}{P_0}\right)^{-1} + \sigma\left(\frac{\bar{\rho}}{\hat{\rho}}\right)^{\frac{2}{3}}\right]\hat{\rho}^{-1}\delta(r_{12}) \,. \end{aligned} \tag{2}$$

The first line, the direct interaction, represents a finite-range attraction, with $f(r_{12}/a)$ a normalized Yukawa potential of range a, viz:

$$f(r_{12}/a) = \frac{1}{4\pi a^3}\frac{e^{-r/a}}{r/a} \,. \tag{3}$$

The product $\hat{\rho}^{-1}f$ is thus dimensionless and the normalization is such that

$$\int d^3r_2 \; f(r_{12}/a) = 1 \,. \tag{4}$$

The factor $\frac{1}{2}(1 \mp \xi)\alpha$ specifies the strength of the attraction, the negative sign referring to like (i.e. neutron-neutron or proton-proton) interactions and the plus sign to unlike, neutron-proton interactions.

The second part of $v(r_{12})$ specifies the saturating part of the nucleon-nucleon potential, i.e. the part responsible for the stability of nuclei against collapse. This part is now taken to have zero range, as described by the delta function $\delta(r_{12})$, also normalized so that

$$\int d^3r_2\ \delta(r_{12}) = 1\ . \tag{5}$$

The strength of the saturating part of the interaction is again different for like and unlike pairs of nucleons, as specified by the factor $\frac{1}{2}(1 \mp \zeta)$. The saturating term depends, in addition, on the magnitude of the momentum, p_{12}, between the nucleons, as well as on a mean density $\bar{\rho}$ defined, as in Part I, by

$$\bar{\rho}^{2/3} = \frac{1}{2}\left(\rho_1^{2/3} + \rho_2^{2/3}\right)\ , \tag{6}$$

where ρ_1 and ρ_2 are the relevant neutron or proton densities at points 1 and 2. Because of the δ-function in the interaction these two points coalesce and $\bar{\rho}$ becomes simply ρ_n (or ρ_p) for neutron-neutron (or proton-proton) interactions, but remains a mean neutron-proton density given by

$$\bar{\rho}^{2/3} = \frac{1}{2}\left(\rho_n^{2/3} + \rho_p^{2/3}\right)\ , \tag{7}$$

for neutron-proton interactions.

The momentum dependence resides partly in a repulsion whose strength increases quadratically with p_{12} (the term proportional to β), and partly in an attraction whose strength decreases as $(1/p_{12})$ (the term proportional to γ). The density dependence of the saturating term resides in a repulsion

whose strength increases as $\bar{\rho}^{\frac{2}{3}}$ (the term proportional to σ). For a discussion of these terms consult Part I.

2.2 The simplified Thomas-Fermi energy

The defining equation of the simplified Thomas-Fermi model is the expression for the total energy E of the system, written as a functional of the density distributions $\rho_n(\mathbf{r})$, $\rho_p(\mathbf{r})$ of the N neutrons and Z protons. This energy will be written as an integral over all space of an energy density $\mathcal{E}(\mathbf{r}_1)$, viz:

$$E = \int d^3r_1 \, \mathcal{E}(\mathbf{r}_1) \, , \tag{8}$$

where $\mathcal{E}(r_1)$ consists of a sum of the kinetic energy density of the nucleons, the energy density due to the nucleon-nucleon potential, Eqs.(1,2), and the electrostatic energy density, viz:

$$\mathcal{E} = \mathcal{E}_K + \mathcal{E}_W + \mathcal{E}_C \, . \tag{9}$$

The neutron and proton densities will be specified, as in Part I, by the dimensionless functions $\Psi(\mathbf{r})$ and $\Phi(\mathbf{r})$ according to

$$\rho_n(\mathbf{r}) = \hat{\rho}\Phi^3(\mathbf{r}) \, , \quad \rho_p(\mathbf{r}) = \hat{\rho}\Psi^3(\mathbf{r}) \, , \tag{10}$$

where $\hat{\rho} = \rho_0/2$ and ρ_0 is related to the nuclear radius constant r_0 by the expression

$$\rho_0 = \left(\frac{4}{3}\pi r_0^3\right)^{-1} \, . \tag{11}$$

As is readily verified, Φ and Ψ represent the local Fermi momenta of the neutrons and protons, P_n and P_p, in units of the Fermi momentum P_0 of

standard nuclear matter, viz:

$$\Phi = P_n/P_0\,, \qquad \Psi = P_p/P_0\,. \tag{12}$$

In terms of these quantities we find the following expressions for the energy densities:

$$\mathcal{E}_K(\mathbf{r}_1)/T_o\hat{\rho} = \frac{3}{5}\left(\Phi_1^5 + \Psi_1^5\right) \tag{13}$$

$$\begin{aligned}\mathcal{E}_W(\mathbf{r}_1)/T_o\hat{\rho} = & -\int d^3r_2\, f(r_{12}/a)\left[\frac{1}{2}\alpha_\ell\left(\Phi_1^3\Phi_2^3 + \Psi_1^3\Psi_2^3\right) + \alpha_u\Phi_1^3\Psi_2^3\right] \\ & + \frac{3}{5}B_\ell\left(\Phi_1^8 + \Psi_1^8\right) - \frac{3}{5}\gamma_\ell\left(\Phi_1^5 + \Psi_1^5\right) \\ & + \frac{3}{5}B_u\Phi_1^3\Psi_1^3\left(\Phi_1^2 + \Psi_1^2\right) - \frac{3}{2}\gamma_u\, X_>^{-1}\left[1 - \frac{1}{5}\frac{X_<^2}{X_>^2}\right]\end{aligned} \tag{14}$$

$$\mathcal{E}_C(\mathbf{r}_1) = \frac{1}{2}\,\mathrm{e}^2\,\hat{\rho}^2\int d^3r_2\,\frac{\Psi_1^3\Psi_2^3}{r_{12}}\,. \tag{15}$$

Eq.(13) expresses the proportionality of the kinetic energy density of a Fermi gas to the five thirds power of the density , i.e. to the fifth power of the Fermi momentum. (In what follows Φ_1 stands for $\Phi(\mathbf{r}_1)$, Φ_2 for $\Phi(\mathbf{r}_2)$, and similarly for Ψ_1 and Ψ_2). The first line in Eq.(14) comes from the finite-range part of the nucleon-nucleon potential (the direct part), the second line from the saturating forces between like nucleons and the third line from the saturating forces between unlike nucleons.

New strength parameters have been defined as follows:

$$
\begin{aligned}
\alpha_{\ell,u} &= \frac{1}{2}(1 \mp \xi)\alpha \\
\beta_{\ell,u} &= \frac{1}{2}(1 \mp \zeta)\beta \\
\gamma_{\ell,u} &= \frac{1}{2}(1 \mp \zeta)\gamma \\
\sigma_{\ell,u} &= \frac{1}{2}(1 \mp \zeta)\sigma \\
B_{\ell,u} &= \sigma_{\ell,u} + \frac{5}{6}\sigma_{\ell,u} \, .
\end{aligned}
\tag{16}
$$

The quantity $X_>$ stands for "the greater of Φ_1 and Ψ_1" and $X_<$ for "the lesser of Φ_1 and Ψ_1". The above expression for $\mathcal{E}_W$ follows from summing the interactions of a nucleon with its neighbors, which implies integrations over the relative distances and relative momenta of all the other nucleons. These integrations are explained in Part I in the case when all the effective interactions have a common range. The easiest way of arriving at the simplified Eq.(14) is to start with the expression for $\mathcal{E}$ in Eq.(17) in Part I and to replace the Yukawa form factor f by a delta function in the saturating terms. Note that when writing the final draft of Part I, we presented Eqs.(17,86) for the energy density in a form where the integrands are not symmetric in the subscripts 1 and 2. The proper symmetric version (actually used by us) is recovered by replacing, in the coefficients of B_ℓ and B_u, the quantity Φ_1^2 by $\frac{1}{2}(\Phi_1^2 + \Phi_2^2)$ and Ψ_1^2 by $\frac{1}{2}(\Psi_1^2 + \Psi_2^2)$. (Note also the following misprints in Part I: In Eq.(72), p_{12} should read p_{12}^2. In Eq.(74), p should read p^2. In the last line of Eq.(80), $\Psi_1^2 + \Psi_1^2$ should read $\Psi_1^2 + \Psi_2^2$.)

We note that the momentum-dependent part of the nucleon-nucleon in-

teraction proportional to β and the density-dependent part proportional to σ, combine to give a contribution to the energy density proportional to $B = \beta + \frac{5}{6}\sigma$. It follows that all predictions of the model as regards energies and density distributions cannot distinguish between different choices of β and σ, provided the sum $\beta + \frac{5}{6}\sigma$ is kept fixed. This degeneracy is broken when the energy dependence of the nuclear optical potential is brought into the discussion (see Part I).

In Eq.(15), e^2 is the square of the proton charge.

2.3 Uniform nuclear matter

For uniform nuclear matter (with any values of the constant neutron and proton densities) integrations over a normalized Yukawa or a normalized delta function form factor give identical results. Hence all the formulae and figures in Sections 4 and 5 in Part I remain unchanged. This is also true of all formulae in Section 8, Part I, describing the potential of a neutron or proton traveling through uniform nuclear matter. In particular Fig. 8 in Part I and the associated discussion of the nuclear optical model potential are unchanged.

2.4 The nuclear potential inside a finite nucleus

By contrast, for a finite nuclear system, the potential U_n or U_p felt by a neutron or proton is now a different function of the nucleon's momentum p

and location r. Thus, by replacing f by a delta function in the saturating terms in Eqs.(76, 77) in Section 12, Part I, we find the simplified expressions

$$U_n(\mathbf{r}_1,\phi)/T_0 = -\int d^3r_2\, f(r_{12}/a)\,\left(\alpha_\ell\Phi_2^3+\alpha_u\Psi_2^3\right) \tag{17}$$

$$+\beta_\ell\left(\frac{3}{5}\Phi_1^5+\Phi_1^3\phi^2\right)+\frac{4}{3}\sigma_\ell\Phi_1^5-\gamma_\ell\left\langle\begin{array}{l}\Phi_1^3\phi^{-1}\\ \Phi_1^2\left[\frac{3}{2}-\frac{1}{2}(\phi/\Phi_1)^2\right]\end{array}\right.$$

$$+\beta_u\left(\frac{3}{5}\Psi_1^5+\Psi_1^3\phi^2\right)+\sigma_u\left(\frac{5}{6}\Psi_1^3\Phi_1^2+\frac{1}{2}\Psi_1^2\right)-\gamma_u\left\langle\begin{array}{l}\Psi_1^3\phi^{-1}\\ \Psi_1^2\left[\frac{3}{2}-\frac{1}{2}(\phi/\Psi_1)^2\right]\end{array}\right. .$$

The proton potential $U_p(r,\psi)$ is obtained by replacing Ψ, ψ with Φ, ϕ.

In the above, ϕ or ψ denote the neutron or proton momentum at the point r_1 in units of P_0. In the terms multiplying γ_ℓ or γ_u in Eq.(17) the upper lines are to be used if ϕ is greater than Φ_1 or Ψ_1, respectively, and the lower line otherwise. A corresponding rule applies in the case of U_p. For a neutron with a momentum equal to the local neutron Fermi momentum, i.e. for $\phi=\Phi_1$, we have (in place of Eq.(78) in Part I):

$$U_n(r_1,\Phi_1)/T_0 = -\int d^3r_2\, f(r_{12}/a)\,\left(\alpha_\ell\Phi_2^3+\alpha_u\Psi_2^3\right)+\frac{8}{5}B_\ell\Phi_1^5-\gamma_\ell\Phi_1^2$$

$$+B_u\left(\frac{3}{5}\Psi_1^5+\Psi_1^3\Phi_1^2\right)-\gamma_u\left\langle\begin{array}{l}\Psi_1^3\Phi_1^{-1}\\ \Psi_1^2\left[\frac{3}{2}-\frac{1}{2}(\Phi_1/\Psi_2)^2\right]\end{array}\right. . \tag{18}$$

In the case of a proton with $\psi=\Psi_1$, the corresponding expression for $U_p(r_1,\Psi_1)$ is obtained by interchanging Φ and Ψ. In these special cases we again find that only the combinations of $\beta_{\ell,u}$ and $\sigma_{\ell,u}$ denoted by $B_{\ell,u}$ appear. Thus the degeneracy between β and σ is perfect not only for predictions of the model regarding energies and density distributions, but also regarding the

potential felt by a neutron or proton at the top of its local Fermi sphere even in the case of non-uniform systems. To break the degeneracy the potential experienced by a nucleon not at its local Fermi momentum must be involved.

2.5 The Euler equations

The Euler equations, two in number, express the condition for the energy of the system to be stationary with respect to infinitesimal particle-preserving density variations $\delta\rho_n$ and $\delta\rho_p$. The result of taking the variation of a kinetic energy density (proportional to Φ^5) with respect to the density (proportional to Φ^3) is proportional to Φ^2. The result of a functional variation of the interaction energy density with respect to the neutron density is the potential experienced by a neutron at the top of its (local) Fermi sphere as given by Eq.(18). Equating the sum of these variations to a constant Lagrange multiplier, we find

$$\Lambda_n = \Phi_1^2 + U_n(r_1, \Phi_1)/T_0\,, \tag{19}$$

$$\Lambda_p = \Psi_1^2 + U_p(r_1, \Psi_1)/T_0\,,$$

where Λ_n, Λ_p are the Lagrange multipliers in units of T_0. Using the equations for U_n and U_p and rearranging terms, Eqs.(19) may be written as polynomials in Φ_1 and Ψ_1 as follows:

$$A_n\Phi_1^5 + B_n\Phi_1^2 + C_n + D_n\Phi_1^{-1} = 0\,, \tag{20}$$

$$A_p\Psi_1^5 + B_p\Psi_1^2 + C_p + D_p\Psi_1^{-1} = 0\,,$$

where the coefficients $A_n ... D_p$ are themselves functions or functionals of Φ and Ψ, given explicitly in Appendix A. The above coupled integral equations are solved by numerical iteration, as described in that Appendix.

2.6 Estimating the adjustable parameters

The present simplified Thomas-Fermi model has the same number of adjustable parameters (seven) as the model in Part I. They are the relative strength parameters $\alpha, \beta, \gamma, \sigma, \xi, \zeta$ and the range a of the finite-range part of the nucleon-nucleon potential. As before, for the purposes of discussing binding energies and density distributions (but not optical model potentials) the parameters β and σ collapse into the single parameter $B = \beta + \frac{5}{6}\sigma$, and there are thus six parameters left: $\alpha, B, \gamma, \xi, \zeta, a$. They may be used to fit six nuclear properties, for example the volume, surface and symmetry energy coefficients a_1, a_2 and J, respectively; nuclear sizes as characterized by the nuclear radius constant r_0 of standard nuclear matter; the width b (i.e. the diffuseness) of the nuclear surface and, finally, the estimated binding of neutron matter [6]. If the diffuseness b is provisionally left out of the fit, five parameters are sufficient: in particular, the parameter γ may be set equal to zero. In that case if, in addition to keeping the constraint on the binding of neutron matter, one picks a value of the radius constant r_0 and fits the predictions of the Thomas-Fermi model, thus constrained, to nuclear binding energies, one comes back with estimated values of a_1, a_2 and J that ensure the best fit to nuclear masses for the given r_0.

A series of such fits was performed by P. Möller with the original Thomas-Fermi model of Part I, using measured binding energies corrected for shell and odd-even effects, as well as for the congruence energy—a form of "Wigner term"—described in Part I, Section 9. The result is shown in Fig. 1, where the output values of a_1, a_2 and J are plotted against the input value of r_0 used in the fit. Even though this plot was obtained with a specific version of the Thomas-Fermi model (the original version, with γ set equal to zero) we expect that also the present version will reproduce approximately nuclear binding energies, provided its parameters are made to reproduce, for a given r_0, the values of a_1, a_2 and J implied by Fig. 1. This is because the four primary "liquid drop" nuclear properties associated with the parameters r_0, a_1, a_2, J are known to be adequate for an approximate representation of nuclear binding energies. Since it turns out to be much easier to determine the parameters of a Thomas-Fermi model that respects the constraint represented by Fig. 1 (together with the constraint on neutron matter binding) than it is to re-fit hundreds of measured binding energies, we have used the above scheme to investigate the effect of varying the sixth parameter of our model (i.e. γ or, in effect, b) under the constraint of approximate agreement with measured binding energies of nuclei and with the estimated binding energy of neutron matter. (For the sake of brevity we shall refer to these constraints collectively as the "binding energy constraint.")

As a preliminary study we investigated the properties of a series of Thomas-Fermi models that include situations intermediate between the original model

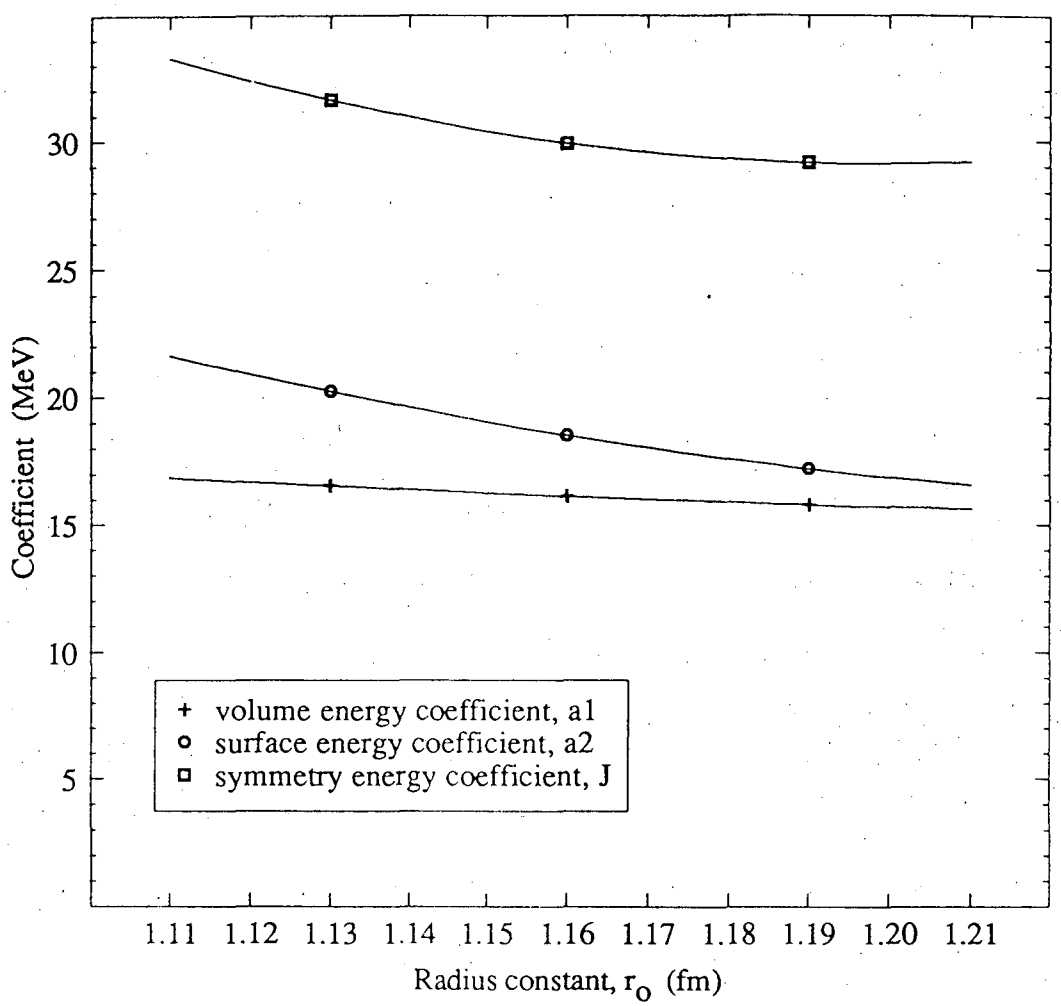

Figure 1: When the Thomas-Fermi model of Part I, with a pre-assigned value of r_0 (and with γ set equal to zero) is fitted to nuclear binding energies and the estimated energy of neutron matter, one finds the nuclear volume, surface and symmetry energy coefficients to have the values shown in a plot versus r_0.

(with equal ranges in all parts of the effective interactions) and the present model with zero range in the saturating part. Fig. 2 shows one aspect of such generalized models, where the range of the saturating Yukawa potential was varied from $a_{\text{sat}} = 0.8$ down to $a_{\text{sat}} = 0$. In all cases γ was set to zero, r_0 was taken to be 1.16 fm, and the other parameters were adjusted according to the scheme explained above, so that $a_1 = 16.12337$ MeV, $a_2 = 18.50754$ MeV and $J = 29.92577$ MeV. It is seen from Fig. 2 that under the abovementioned binding energy constraint a reduction of the range of the saturating terms calls for a reduction also in the range of the direct attraction. The calculated diffuseness of a plane surface of semi-infinite nuclear matter, as characterized by the width b_0, is seen to increase somewhat from about 0.8 fm when $a_{\text{sat}} = a \approx 0.57$ to about 0.97 fm when $a_{\text{sat}} = 0$. It was partly because short-range saturating terms are, perhaps, more reasonable on physical grounds, partly because a somewhat larger diffuseness is indicated by measurements, and partly because the resulting model is simpler algebraically, that we changed from the original to the present model.

Table I lists a set of parameters of the present model (with $a_{\text{sat}} = 0$) for three choices of r_0. The binding properties were fitted (approximately) as explained above and, by adjusting γ, the surface width b_0 of semi-infinite nuclear matter was made equal to 1.1 fm, a value yielding approximate agreement with measurements. These three sets of parameters can now be used to confront the predictions of the present model with nuclear fission barriers and charge distributions.

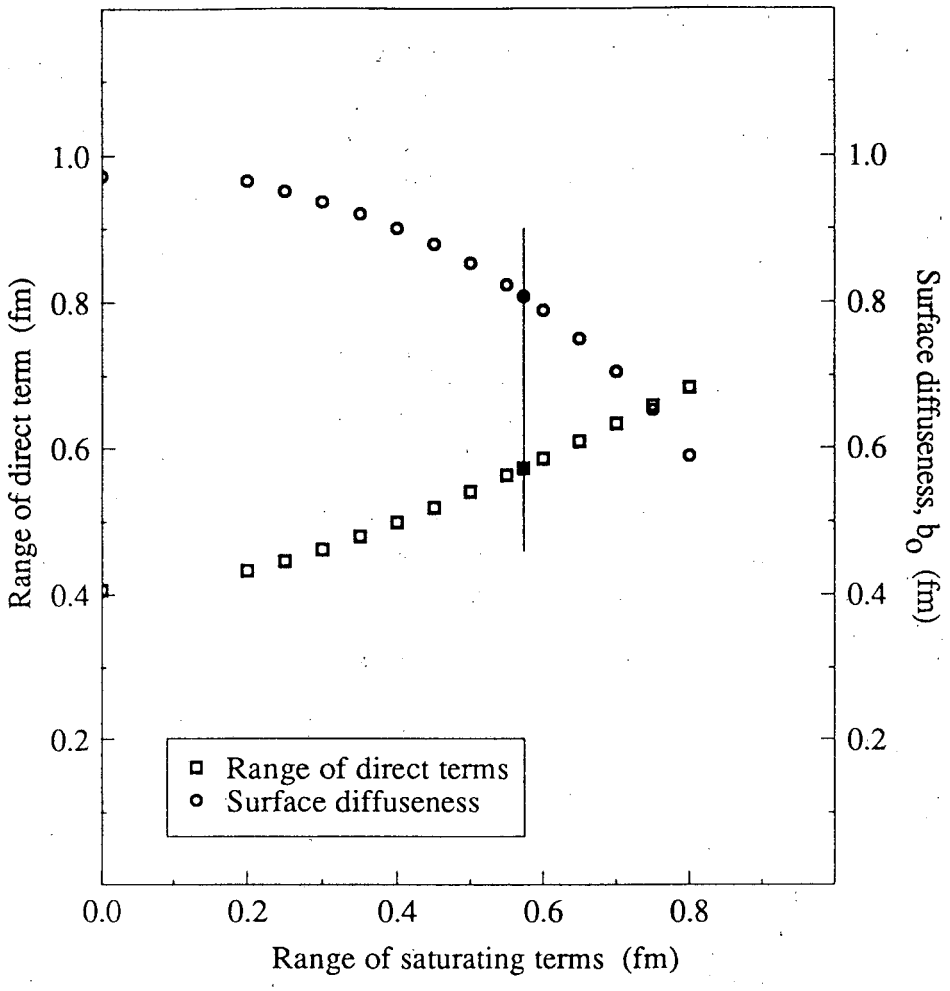

Figure 2: A study of generalized models where the saturating and direct parts of the effective nucleon-nucleon interactions have different ranges. These models all have $\gamma = 0$, $r_0 = 1.16$ fm and are constrained to reproduce nuclear binding energies as in Fig. 1. The vertical bar corresponds to the model of Part I, where the saturating and direct ranges are equal.

Table I: Parameter sets used in the calculations.

	Value of the radius constant, r_0 (fm)		
	1.13	1.16	1.19
Mass fit[a] (MeV)			
a_1	16.53900	16.12337	15.78722
a_2	20.23740	18.50754	17.20108
J	31.63260	29.92577	29.16030
Additional constraint (fm)			
b_0	1.1	1.1	1.1
Interaction parameters			
α	3.21227	3.00401	2.87973
B	1.38002	1.33549	1.31623
γ	0.43471	0.58372	0.69091
ξ	0.42392	0.42667	0.42154
ζ	0.60820	0.65127	0.65504
a (fm)	0.49030	0.50614	0.51935
Droplet Model quantities (MeV)			
K	286.45	268.62	255.72
L	46.05	37.22	35.79
M	6.10	6.40	6.41
Q	37.22	41.32	42.96
a_3	11.01	9.83	8.93
Related quantities			
ρ_0 (fm^{-3})	0.16545	0.15295	0.14167
T_f (MeV)	37.67873	35.75502	33.97497
P_f (MeV/c)	265.9983	259.1190	252.5966
Additional fit parameters[a] (MeV)			
W	30[b]	33.41818	28.27983
a_0	-16.77100	-10.94316	-6.35519

[a] From Peter Möller [7].
[b] Constrained value.

3 Fission Barriers

The determination of the equilibrium configuration and energy of a non-spherical nucleus is considerably more difficult, since the functions Φ and Ψ in the Euler equations depend now on three position coordinates x, y, z rather than on the radial distance r only. The technique for solving this problem numerically on a three-dimensional lattice (without parameterizing Φ and Ψ in any way) is described in Appendix B.

Fig. 3 shows the result of fission barrier calculations for five nuclei, with atomic numbers Z=70, 80, 93, 100 and 108. The set of parameters corresponding to $r_0 = 1.16$ in Table I was used. For each nucleus the equilibrium configuration was determined under the constraint that the distance between the centers of mass of the two halves of the (reflection symmetric) system, denoted by $2 < z >$, should have a pre-assigned value. The energy of such a conditional equilibrium shape is plotted against Δ, the excess of $< z >$ over its value $< z >_0$ for the spherical (unconstrained) configuration. The maximum in the resulting curve corresponds to the height of the fission barrier for the given nucleus. In the case of Z=70 and 80 the continuation of the calculations beyond the maximum can be seen to lead eventually to a point where the family of conditional equilibrium solutions comes to an end (in a plot vs. Δ). The numerical iterative search for a solution does, nevertheless, automatically home in on another branch of conditional equilibrium configurations, those corresponding to the 'fusion valley' where two fragments

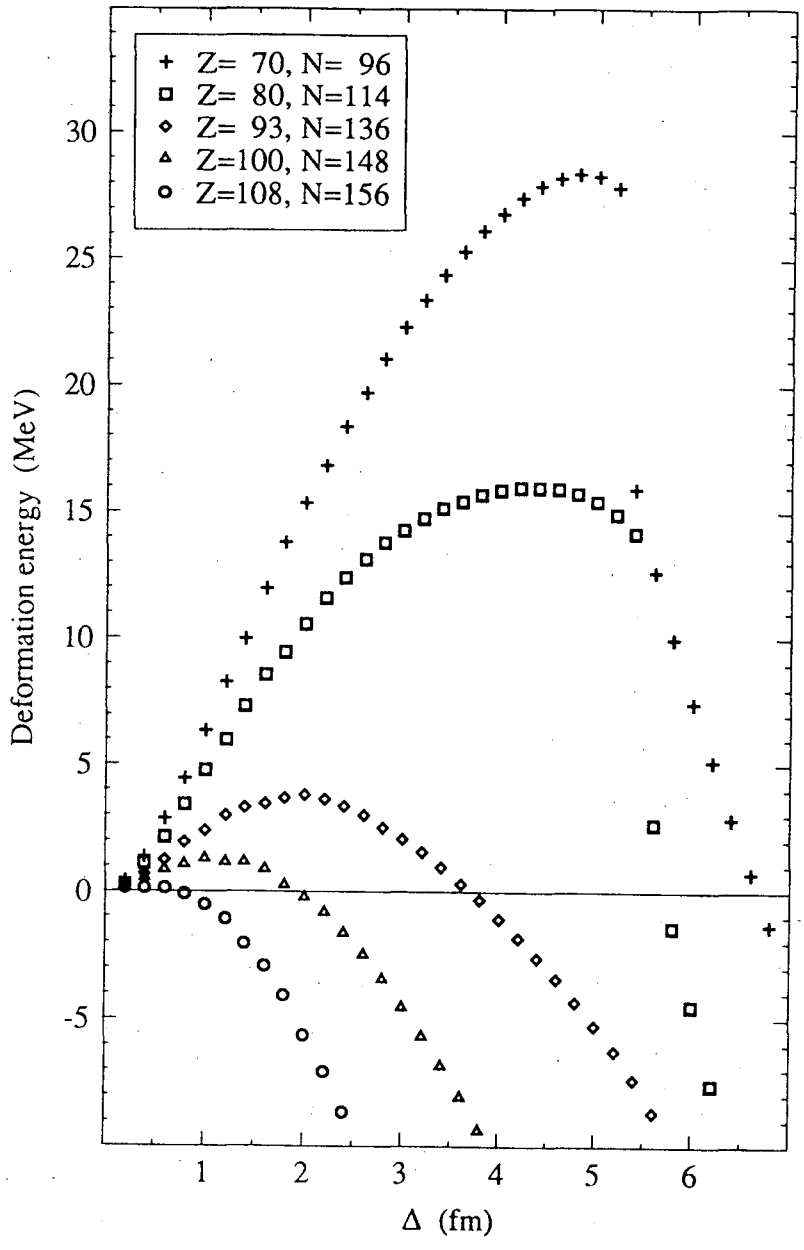

Figure 3: Calculated deformation energies of conditional equilibrium shapes for five nuclei. The constraint parameter Δ is half the distance between the centers of mass of the two halves of the nuclear shape, less its value for the spherical configuration. The maximum in each curve corresponds to the fission barrier height. The break in the two upper curves corresponds to the point where the family of conditional equilibrium shapes comes to an end (by bending back at a limiting point). The continuation of this family (not shown) goes through another bend and re-emerges as the "fusion valley" of two separated fragments with a constrained center-of-mass separation. Our iterative solutions of the Euler equations home in on this valley and trace out its energy which, apart from some fragment deformation, corresponds simply to the Coulomb interaction between the fragments.

Table II: Experimental and calculated fission barriers.

		Experimental (MeV)	Calculated (MeV)		
			Value of the radius constant, r_0 (fm)		
Z	N		1.13	1.16	1.19
70	96	24.20[b]		28.4 (2.51)[a]	
80	114	13.73[b]	25.1 (2.58)	16.0 (2.64)	
93	136	3.78[b]	8.3 (2.72)	3.8 (2.79)	1.7 (2.86)
100	148	1.5[c]		1.3 (2.87)	
108	156	0.3[c]		0.2 (2.93)	

[a] Numbers in parentheses refer to $< z >_0$, where $2 < z >_0$ is the distance in fermis between the centers of mass of the two halves of the spherical density distributions for the nucleus in question.
[b] Ref.[8]. Strictly speaking these are not experimental values, but values calculated by Sierk using a model [9] which (when combined with shell effects) is known to give good agreement with experiment.
[c] Ref.[10].

(somewhat flattened by the Coulomb repulsion) are held at the pre-assigned center-of mass separation. Fig. 4 depicts the appearance of three of the saddle-point shapes from Fig. 3. The first part is a three-dimensional rendering and the others are plots of the contours of the neutron densities. Fig. 5 shows three barrier calculations for $Z = 93$, $N = 136$ using the parameter sets for $r_0 = 1.13, 1.16, 1.19$, to be discussed presently. Similarly, Fig. 6 shows the barrier calculation for ^{194}Hg ($Z = 80$, $N = 114$) using the parameter sets for r_0 =1.13 and 1.16. Table II summarizes the calculated barrier heights and compares them with values deduced from experiment. By taking $r_0 = 1.16$ fm the calculated barriers for the heaviest elements can be made to agree with measurements. However, for $Z = 80$ the calculated barrier is some 2 MeV too high and for $Z = 70$ the difference is about 4 MeV.

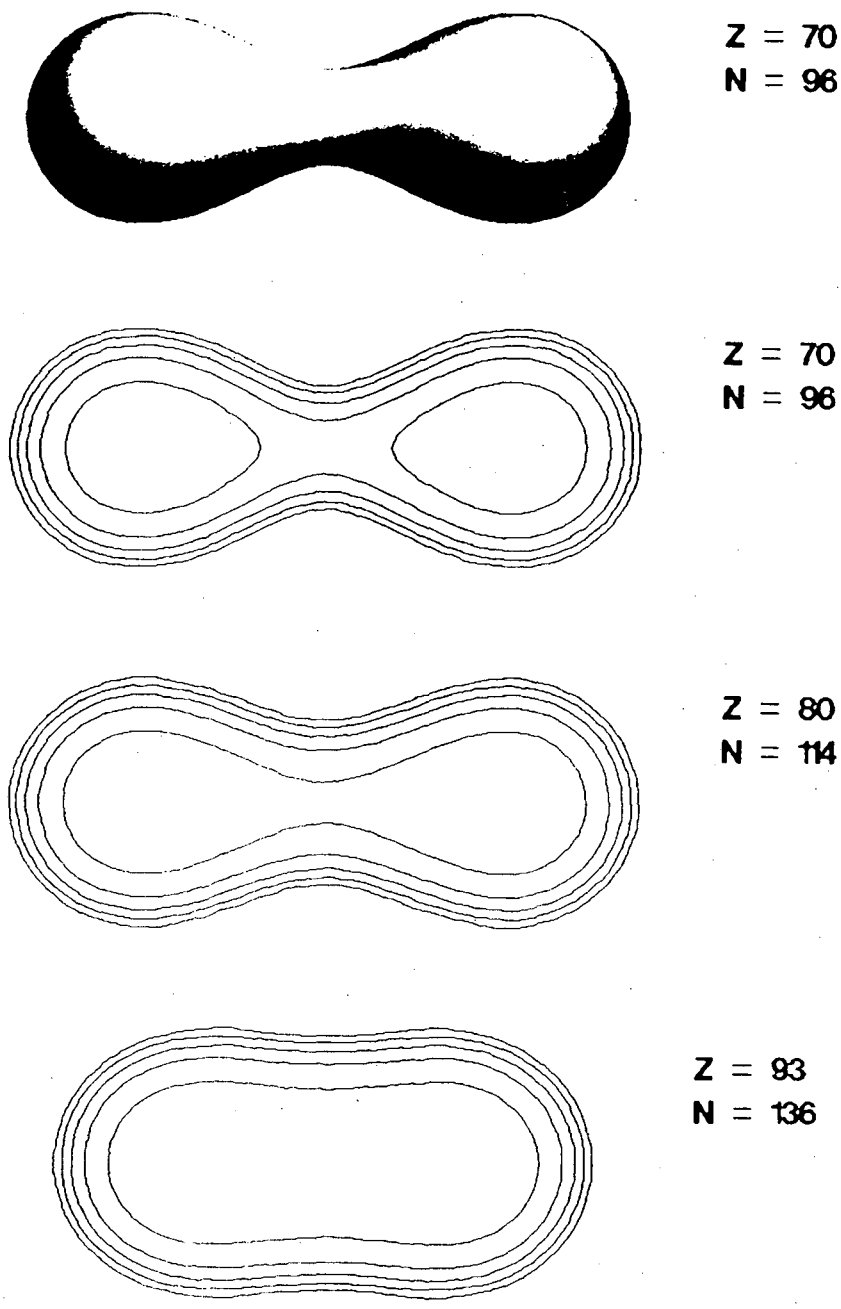

Figure 4: Illustration of the saddle-point shapes for ^{166}Yb, ^{194}Hg and ^{229}Np. The upper part of the figure is a three-dimensional rendering and the plots below are contour lines of the neutron density corresponding to $\rho_n/\hat{\rho} = 0.2, 0.4, 0.6, 0.8, 1.0$.

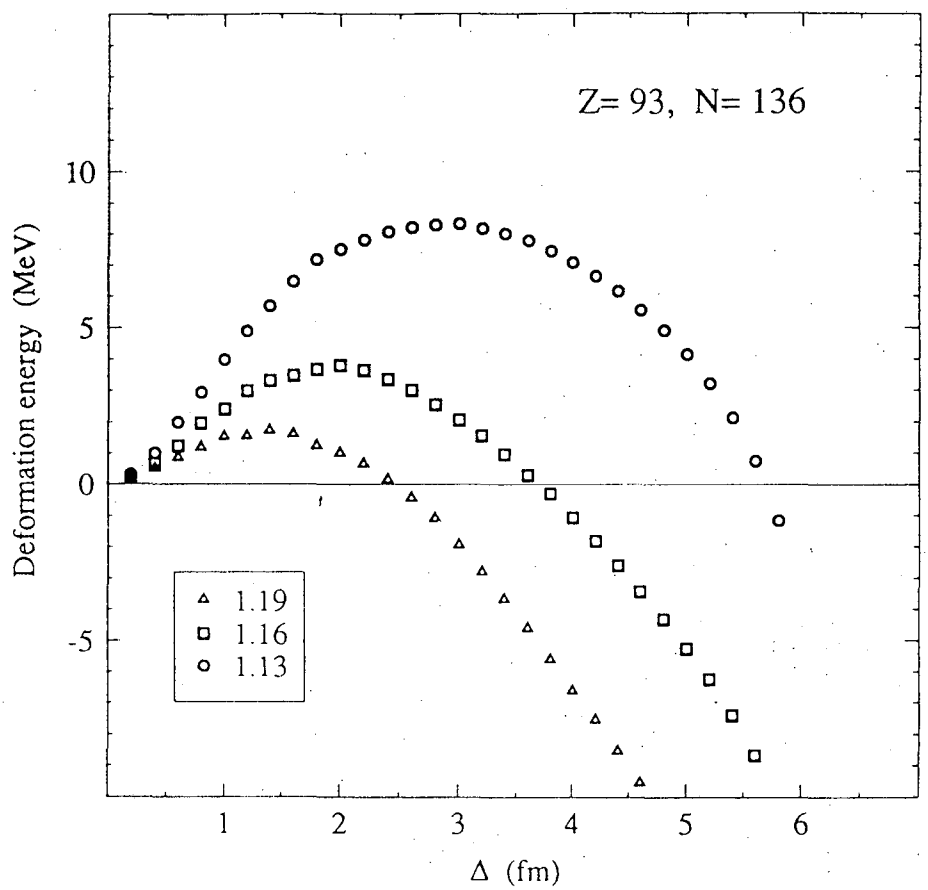

Figure 5: This figure shows the fission barrier plots for the nucleus ^{229}Np. It illustrates the effect on the barrier height of changing the radius parameter r_0 while (approximately) preserving the fit to ground state masses. (The three parameter sets from Table I were used.)

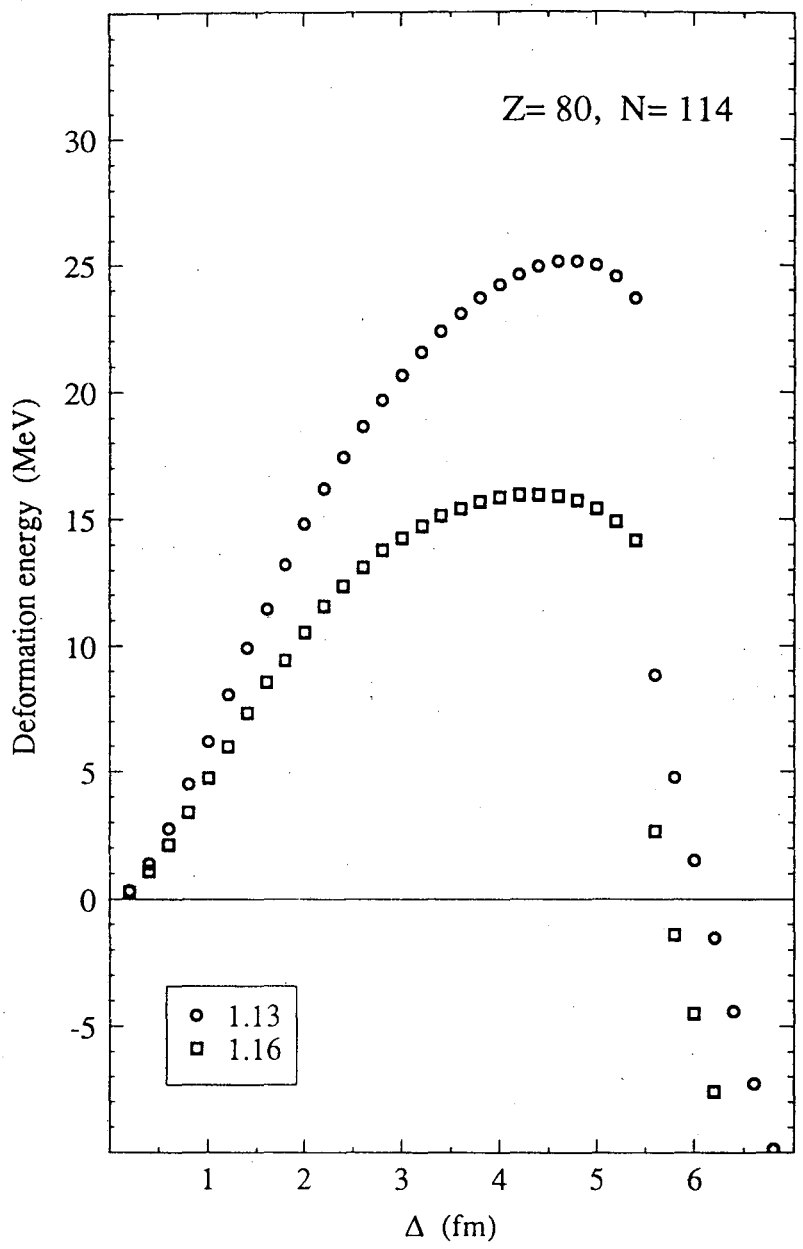

Figure 6: This shows the effect of changing r_0 from 1.13 fm to 1.16 fm in the case of the nucleus ^{194}Hg.

Part of this discrepancy could possibly be due to the implicit assumption in these calculations that the congruence energy, included in the binding energy calculations, i.e.

$$E_{\text{con}} = a_0 + W|I| \tag{21}$$

does not change at all with deformation until after the top of the fission barrier. This cannot be quite correct. According to our interpretation of the congruence energy [11], its value has to double in the course of a division of a nucleus into two parts, and some of this change has presumably already occurred at the top of the fission barrier. Unfortunately, the precise deformation dependence of the congruence energy is still an unsolved problem. We believe that most of the change occurs near scission and is associated with the loss of communication between the two nascent fission fragments [12]. As an illustrative rough estimate let us then assume that a measure of this communication is given approximately by the density ρ_c at the center of the neck between the fragments, i.e. at the origin of coordinates located at the mid-plane of the reflection symmetric shapes. This central neck density will depend on the value of the deformation constraint Δ, and will undergo a rather rapid drop from its original value to zero around scission.

A term of the form

$$(a_0 + W|I|)\left[2 - \frac{\rho_c(\Delta)}{\rho_c(0)}\right] \tag{22}$$

starts off with the value $a_0+W|I|$ for the spherical shape, when $\rho_c(\Delta) = \rho_c(0)$, and doubles to $2(a_0 + W|I|)$ after scission, as required. Fig. 7 shows

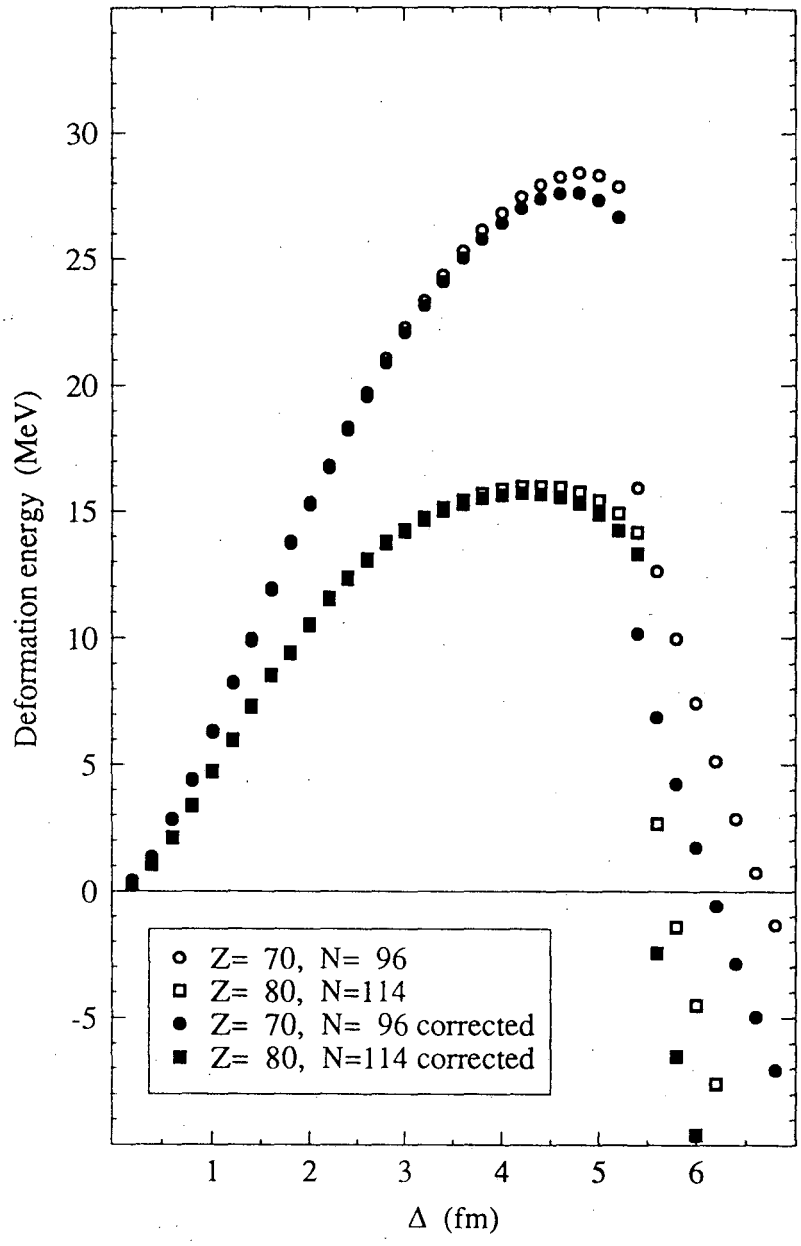

Figure 7: This figure illustrates one attempt to include the effect of the shape dependence of the congruence energy, $a_0 + W|I|$, on the fission barriers for ^{166}Yb and ^{194}Hg. With the assumed shape dependence, the effect on the barriers is small. (These plots correspond to a radius constant $r_0 = 1.16$ fm.)

the fission barrier calculations for ^{166}Yb and ^{194}Hg with and without such a shape-dependence of the congruence energy. The calculated barriers are lowered by about 1 and $\frac{1}{2}$ MeV, respectively. For the heavier nuclei, when $\rho_c/\rho_c(0)$ is close to 1 for the compact saddle point shapes in question, the barriers remain practically unaffected. Unless the shape dependence of the congruence energy has been grossly misrepresented in the above estimate— and this cannot be excluded— it would seem that this modification does not remove the discrepancy. As things stand, the fission barriers of the lighter elements cannot be reproduced even when the barriers for the heavy elements have been fitted (by adjusting r_0 to have the value 1.16 fm). In fact, however, the discrepancy is worse than that: the choice $r_0 = 1.16$ fm is unacceptable when the corresponding calculated charge distributions are compared with measurements.

4 Charge Distributions

Fig. 8 compares the measured charge distributions for ^{56}Fe, ^{124}Su, ^{208}Bi with calculations in which $r_0 = 1.16$ fm was used, together with the associated parameter set from Table I. The calculated curves have the charge distribution of the proton folded in, with an RMS radius of 0.85 fm (and a Yukawa form factor). The pair of measured distributions displayed by solid lines represent parameterized two- and three-parameter fits to electron scattering data [13]. It is clear that the calculated distributions are systematically too low in the bulk and have somewhat too large effective radii. Fig. 9 shows a similar comparison when $r_0 = 1.13$ fm is used, along with its parameter set. The bulk densities and radii are now in fair agreement, although the details (e.g. the fall-off profile in the surface) are still not reproduced. Taking the $r_0 = 1.13$ fm parameter set and recalculating the fission barriers, now leads to disaster: the barrier for the nucleus $Z = 93$, $N = 136$ comes out to be 8.3 MeV instead of 3.8 MeV. Similarly for $Z = 80$, $N = 114$ we find 25.1 MeV where measurements indicated 13.7 MeV. (See Figs. 5,6 and Table II.) Thus we have a clear-cut discrepancy: using a Thomas-Fermi model adjusted to reproduce nuclear binding energies, a choice of r_0 equal to 1.13 fm can reproduce nuclear sizes but not fission barriers. The choice $r_0 = 1.16$ fm would reproduce at least the barriers for heavy elements, but this value is simply not in agreement with measured sizes of nuclei. Using the measured value of r_0, the calculated fission barriers are too high.

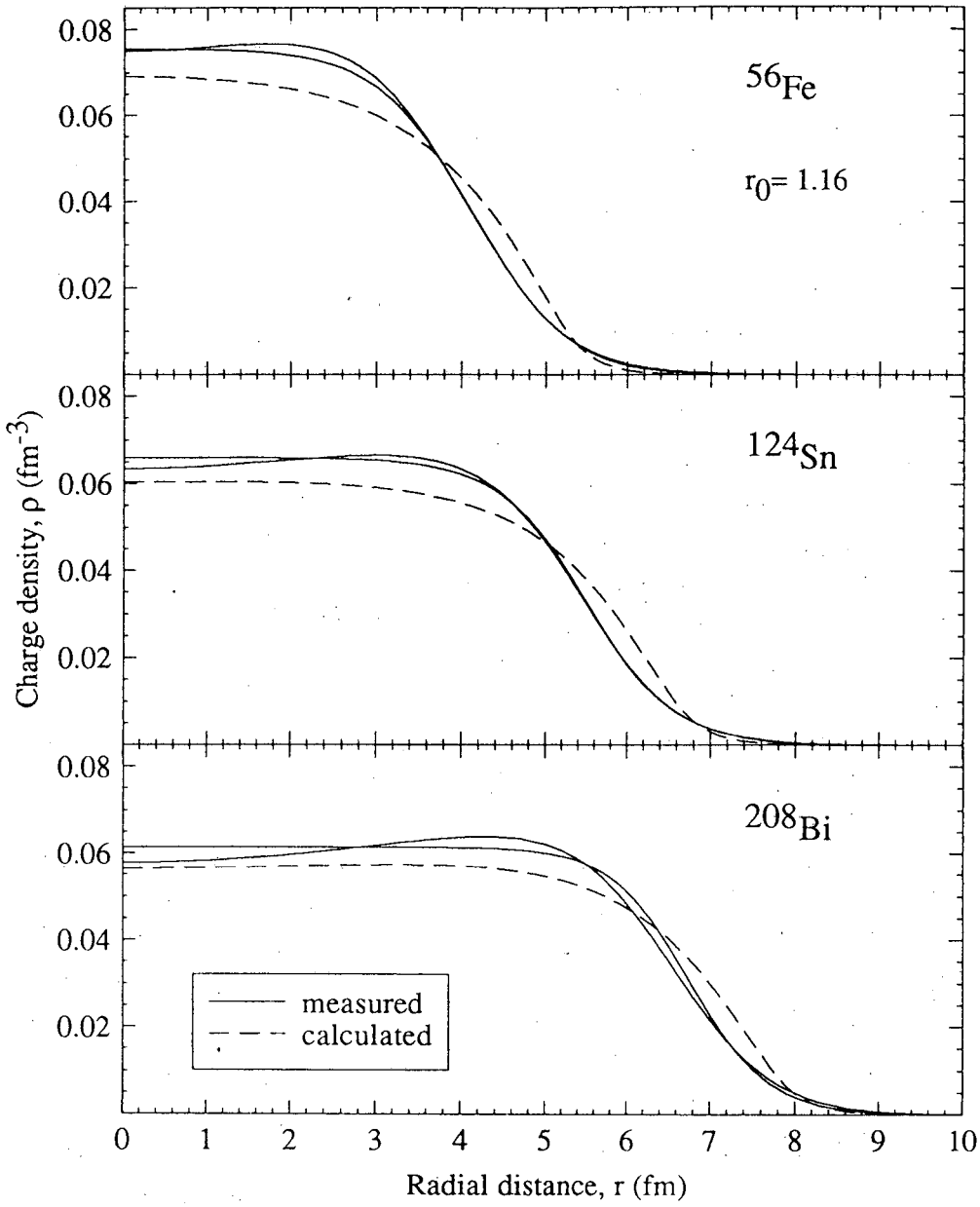

Figure 8: The solid curves correspond to the measured charge distributions, as parameterized by a two-parameter Woods-Saxon form factor, or a "three parameter Gaussian" form factor. The latter curves show a central depression in the charge distribution. The dashed curves correspond to the Thomas-Fermi calculations with the parameter set corresponding to $r_0 = 1.16$. A proton charge form factor (with a Yukawa shape and an RMS size of 0.85 fm) has been folded in.

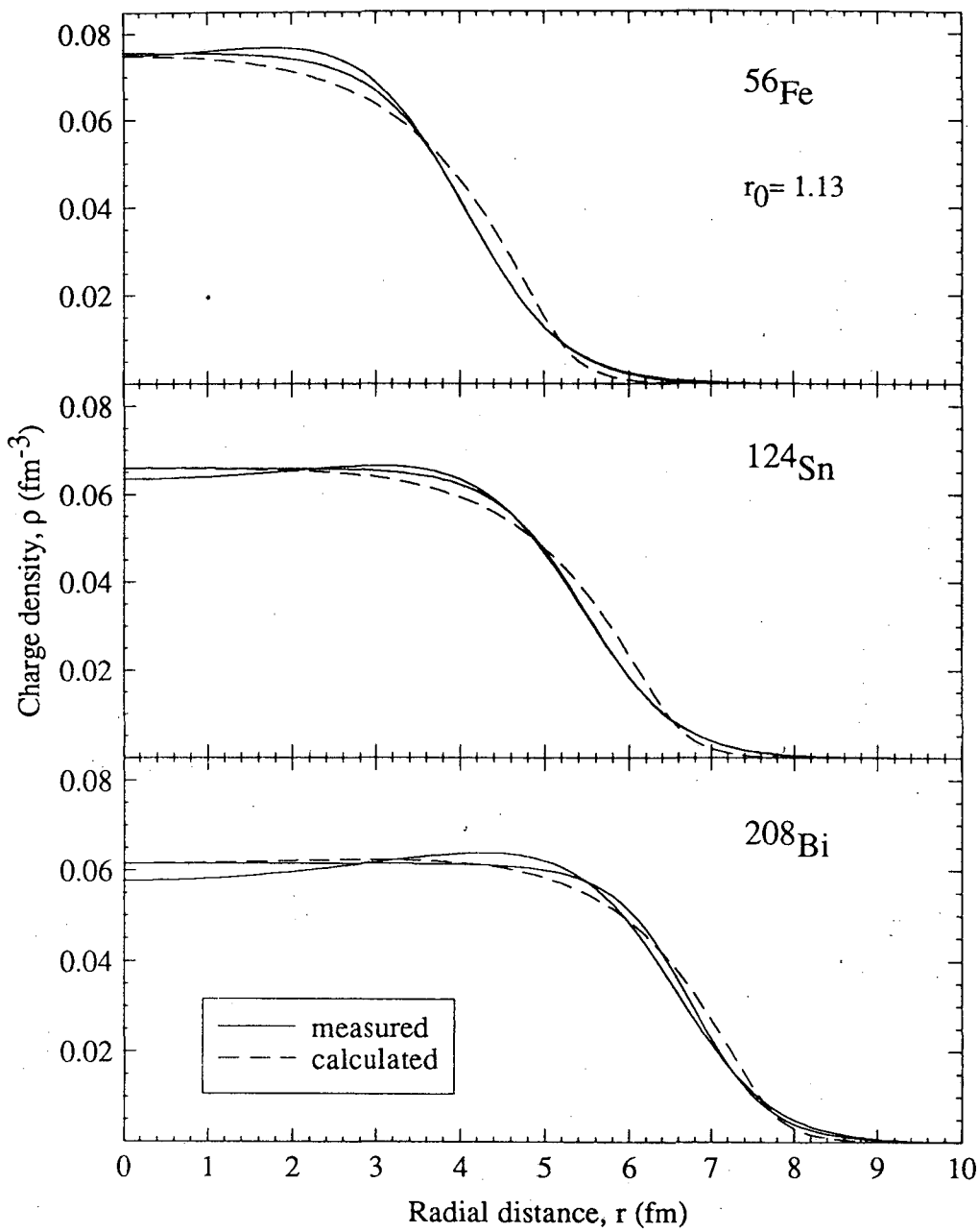

Figure 9: This is like Fig.8, but with the parameter set corresponding to $r_0 = 1.13$.

For related discussions of the fission barrier problem see [9] and [14,15].

5 Discussion

We have explored a number of additional parameter choices and hypotheses in order to test the firmness of the above conclusion, and we believe that, within the framework of the Thomas-Fermi approach, no adjustments of parameters can remove the discrepancy. It is true that, as regards nuclear radii, the discrepancy is no more than about 3%, but the integrity of the model, the accuracy of the unparameterized solutions and the amount of data brought to bear on the determination of the model's parameters are such that we are inclined to consider this discrepancy as the signal of a relatively small but definite piece of physics that is missing in the Thomas-Fermi treatment of average nuclear properties. We regard this as one of the principal conclusions of this work.

The identification of this missing piece of physics is an outstanding problem. We believe the answer may be along the following lines. The Thomas-Fermi treatment is a semi-classical approximation that works well in the bulk region of the nucleus but becomes less accurate in the surface and eventually fails completely in the sense that it allows no penetration of the particles into classically forbidden regions of space. Estimates show that even in heavy nuclei a significant fraction of the nuclear matter finds itself in the classically forbidden region, forming a quantal halo of material contributing positive density but negative kinetic energy density. One anticipated consequence of the presence of a fringe of negative kinetic energy in the outer layers of the

surface is that such a surface should be relatively easier to bend, and the corresponding nucleus should be easier to deform. As a result, the calculated fission barriers should be lowered by the presence of the halo, possibly removing the abovementioned discrepancy. In more technical terms, the presence of the quantal halo should have the effect of reducing the curvature correction to the nuclear surface energy: a convexly curved surface has a relatively greater volume of space available for the energetically favourable quantal halo, and this reduces the opposite effect of curvature, that of decreasing the interaction energy (the result of the increased exposure of particles in the surface region). (For a discussion of a puzzle concerning the status of the curvature energy in nuclear problems, see [16].) In a forthcoming paper we hope to examine the effect of the quantal halo on the size vs. barriers discrepancy uncovered in the present work. We are currently developing a generalization of the Thomas-Fermi model—simpler than conventional refinements [3,17]—designed to accommodate the presence of matter possessing negative kinetic energy.

For some purposes the present unrefined Thomas-Fermi model is expected to remain useful. Thus by considering r_0 to be an adjustable parameter, one may still achieve an adequate description of nuclear masses and deformation energies in a range of conditions much broader than in corresponding Liquid Drop or Droplet Model approaches. The blemish on such a Thomas-Fermi model will be its overestimate of nuclear sizes by about 3%.

6 Appendix A

The coefficients in the Euler Eqs.(20) in Section 2.5 are given by

$$
\begin{aligned}
A_n &= \frac{8}{5}B_\ell\,, \qquad B_n = 1-\gamma_\ell + B_u\Psi_1^3\,,\\
C_n &= -\Lambda_n - \int d^3r_2\, f\,\left(\alpha_\ell\Phi_2^3+\alpha_u\Psi_2^3\right) + \frac{3}{5}B_u\Psi_1^5 - \gamma_u \begin{cases} 0 & \text{if } \Phi_1 > \Psi_1 \\ \frac{3}{2}\Psi_1^2 & \text{if } \Phi_1 < \Psi_1\,, \end{cases}\\
D_n &= -\gamma_u \begin{cases} \Psi_1^3 & \text{if } \Phi_1 > \Psi_1 \\ 0 & \text{if } \Phi_1 < \Psi_1\,, \end{cases}
\end{aligned}
\tag{23}
$$

and

$$
\begin{aligned}
A_p &= \frac{8}{5}B_\ell\,, \qquad B_p = 1-\gamma_\ell + B_u\Phi_1^3\,,\\
C_p &= -\Lambda_p - \int d^3r_2\, f\,\left(\alpha_\ell\Psi_2^3+\alpha_u\Phi_2^3\right) + \frac{3}{5}B_u\Phi_1^5 - \gamma_u \begin{cases} 0 & \text{if } \Psi_1 > \Phi_1 \\ \frac{3}{2}\Phi_1^2 & \text{if } \Psi_1 < \Phi_1 \end{cases}\\
&\quad + e^2\hat{\rho}\int d^3r_2\,\Psi_2^3/r_{12}\,,\\
D_p &= -\gamma_u \begin{cases} \Phi_1^3 & \text{if } \Psi_1 > \Phi_1 \\ 0 & \text{if } \Psi_1 < \Phi_1\,, \end{cases}
\end{aligned}
\tag{24}
$$

Assuming starting estimates for $\Phi(\mathbf{r}_1)$ and $\Psi(\mathbf{r}_1)$ and for the chemical potentials Λ_n and Λ_p, the coefficients $A_n ... D_p$ are calculated at each point $\mathbf{r}_1$ (in the case of C_n and C_p by carrying out numerically the integration over $\mathbf{r}_2$). The polynomial Equations (20) are then solved numerically to obtain intermediate estimates of $\Phi(\mathbf{r}_1)$ and $\Psi(\mathbf{r}_1)$. Since these distributions do not, in general, correspond to the original number of neutrons and protons, the chemical potentials are varied until N and Z agree with the original

choices. The new functions $\Phi(\mathbf{r}_1)$ and $\Psi(\mathbf{r}_1)$ thus obtained constitute the next approximation. The determination of the coefficients $A_n ... D_p$ is now repeated using these functions and the whole procedure is iterated to convergence. The technique is similar to that used in Part I, except that the polynomials (20), which are no longer cubic, are now solved numerically.

7 Appendix B

The assumption of axial symmetry would suffice for the calculation of fission barriers without angular momentum, but in order to allow for the calculation of fission barriers in the presence of angular momentum (work in progress) we have solved the Euler equations (20) on a three-dimensional Cartesian lattice. The problem is thus discretized by the specification of a finite number of values of Φ_{ijk} and Ψ_{ijk} at lattice points located at the (x, y, z) coordinates (ih, jh, kh), where i, j, k are integers and h is the lattice spacing. In what follows we shall specialize to configurations with reflection symmetry about the coordinate planes, so it suffices to specify the densities in an octant for which i, j, k are non-negative integers: $0, 1, 2, 3 \ldots$. Fig. 10 illustrates the nature of this computational space. At each lattice point i, j, k in this figure there is located a small sphere whose radius (for display purposes) was chosen to be proportional to the density at that point. The example shown is for the fission saddle-point neutron distribution of ^{229}Np. (Two other renderings of this density distribution are given in Fig. 4.)

In solving the Euler equations the most time-consuming part of the calculation is the six-layer-deep set of DO loops that are used to calculate the potentials U_n and U_p. Reducing the lattice spacing by a factor of two increases the computation time by a factor of $2^6 = 64$!

Since the practical lower limit of about 0.5 fm for the lattice spacing imposed by this computational constraint is not small compared to the range of

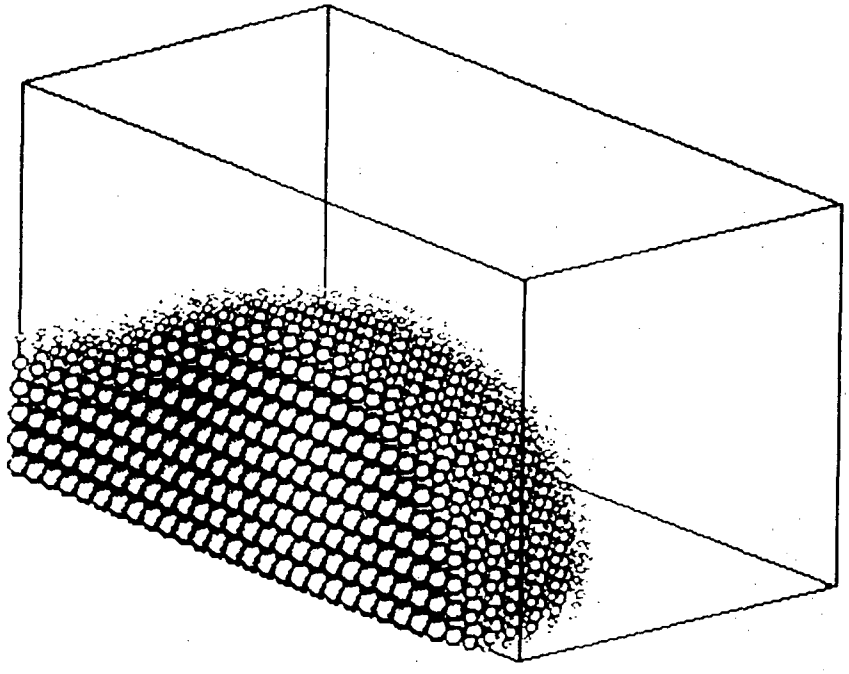

Figure 10: One way of displaying the 3D fission saddle point neutron distribution of ^{229}Np is shown in this figure. In the octant of space actually used in the calculation, a small sphere is located at each lattice site. For display purposes the radii of the spheres were then taken to be proportional to the local density.

the nucleon-nucleon force—in fact the two are comparable—straightforward lowest-order numerical integrations would be quite inaccurate. Higher-order integration formulae in three dimensions are cumbersome and they would have to rely on taking numerical derivatives, with the attendant loss of precision. In view of this we have developed an alternative numerical procedure which, together with two additional tricks, gives accurate results even with the above coarse lattice spacing.

We imagine a (neutron or proton) density distribution $\rho(\mathbf{r})$ to be cut up into little cubes (of volume h^3) centered on the lattice points i, j, k. The amount of matter in each cube is approximated by $h^3\rho_{ijk}$. The total interaction energy of the resulting 'pile of cubes' is now the sum of the self energies of the cubes and of the interaction energies between them. For purposes of calculating the total energy, or the potential in a given cell, imagine the cubes to be replaced by 'equivalent spheres' with radii R chosen to contain the same amount of matter at the (uniform) density ρ_{ijk} as the cubes, so that

$$\frac{4}{3}\pi R^3 = h^3 . \tag{25}$$

Since formulae for the self energy as well as for the mutual interaction energies of uniform spherical distributions of Yukawa matter are known [18,19], the total interaction energy of the pile of equivalent spheres can now be calculated without further approximation.

As regards the calculation of the (average) potentials in the Euler equa-

tions appropriate for each cell i, j, k, the above pile-of-spheres method results in replacing an integral of the type

$$u(\mathbf{r}_1) = \frac{1}{4\pi a^3} \int d^3 r_2 \, \frac{e^{-r_{12}/a}}{r_{12}/a} \, \rho(\mathbf{r}_2) \, , \tag{26}$$

by the expression

$$\begin{aligned} u(\mathbf{r}_1) = & \left[1 - 3\varepsilon^{-3} (\varepsilon \cosh \varepsilon - \sinh \varepsilon)(1+\varepsilon)\mathrm{e}^{-\varepsilon}\right] \rho(\mathbf{r}_1) \\ & + 3\varepsilon^{-3} (\varepsilon \cosh \varepsilon - \sinh \varepsilon)^2 \sum_{\mathbf{r}_2} \frac{e^{-r_{12}/a}}{r_{12}/a} \, \rho(\mathbf{r}_2) \, , \end{aligned} \tag{27}$$

where $\varepsilon = R/a$, and where $\mathbf{r}_1$ identifies the lattice point i, j, k, and the sum over r_2 stands for the sum over contributions to the potential from all the other lattice points i_2, j_2, k_2. The first line is the contribution to the average potential in the cell i, j, k due to the sphere at i, j, k itself. The two lines in Eq.(27) follow from the expressions for the self energy of a spherical distribution of Yukawa matter and from the interaction energy of two such spheres, as given in Refs. [18,19].

The above stratagem of using exact expressions for sphere-sphere interactions allows us to use a rather coarse lattice. The accuracy can be improved further by two additional tricks.

By applying the pile-of-spheres method to the calculation of the binding energy per particle for a sequence of uncharged spherical nuclei with mass number A (and $N = Z$), plotting the results as a function of $A^{-1/3}$, and comparing with similar plots obtained using the very accurate spherically symmetric method (with many more integration points per fermi), one

finds two types of inaccuracies. First, extrapolations of the discrepancies to $A^{-1/3} = 0$, i.e. to the limit of nuclear matter, show that the volume binding energy per particle calculated with the pile-of-spheres method is too strong by a few tenths of a percent. This may be due to the fact that the sphere-sphere formula overestimates slightly the interaction between the six most strongly interacting *adjacent* cubes. This is because adjacent equivalent spheres actually overlap a little and, by deforming them back into non-overlapping cubes, one would expect the interaction to decrease.

Second, from the slopes of the above plots against $A^{-1/3}$, one concludes that the surface energy coefficient is also somewhat overestimated by the pile-of-spheres method. This might be due to the fact that in this method the system's surface is slightly roughed-up by the discretized bumps, the surface thus acquiring some extra diffuseness. In any case, these volume and surface energy discrepancies may be largely removed by using a slightly renormalized strength α' and a slightly renormalized range a' of the Yukawa interaction, written as $\alpha\, f(r_{12})$, where $f(r_{12})$ is given by Eq.(4). By carrying out a series of tests of the pile-of-spheres method for different lattice spacings h, the following empirical correction factors were deduced:

$$\alpha' = \alpha/(1 + k_1(h/a)^2)\,, \tag{28}$$

$$a' = a/(1 + k_2(h/a)^2)\,, \tag{29}$$

where, for the model used in Part I, we found the values $k_1 \approx 0.0062$ and $k_2 \approx 0.05$ to be appropriate. With these correction factors included, the

pile-of-spheres method reproduces the binding energies calculated in Part I to better than 0.1% when $h = 0.6$ fm. This is also the approximate accuracy of the present calculations with $h = 0.5$ fm. Some further improvement might be achieved by re-tuning the values of k_1 and k_2 for optimum performance with the present model. Even without such re-tuning, the amazing success of the pile-of-spheres method for approximating the binding energy of small systems is illustrated in Fig. 11, which represents the results of calculating the binding energy (per particle) of systems with A from 8000 down to 1. The dots represent the more accurate calculations using radial integrations and the circles the discretized calculations on a 0.5 fm lattice. The difference is barely discernible even for $A \approx 1$. (This close correspondence was found to continue to even smaller values of A! Since the Thomas-Fermi model knows nothing about the discreteness of the nucleons, such tests of approximation schemes down to $A \approx 1$ and beyond are not meaningless.)

The solid line corresponds to the equation

$$E/A = -a_1 + a_2 A^{-1/3} + \left(a_3 - \frac{2a_2^2}{K}\right) A^{-2/3} - 22.615 A^{-1} + 10.121 A^{-4/3} . \quad (30)$$

Here the coefficients a_1, a_2, a_3, K were calculated from the properties of infinite or semi-infinite nuclear matter, as listed in Table I, i.e. they were *not* fitted to the points in Fig. 11. The functional form of the first three terms follows the Droplet Model theory [20]. The last two terms, for which no theory is available, were adjusted for a best fit to the dots in Fig. 11. The virtually perfect fit confirms the usefulness of a leptodermous expansion of

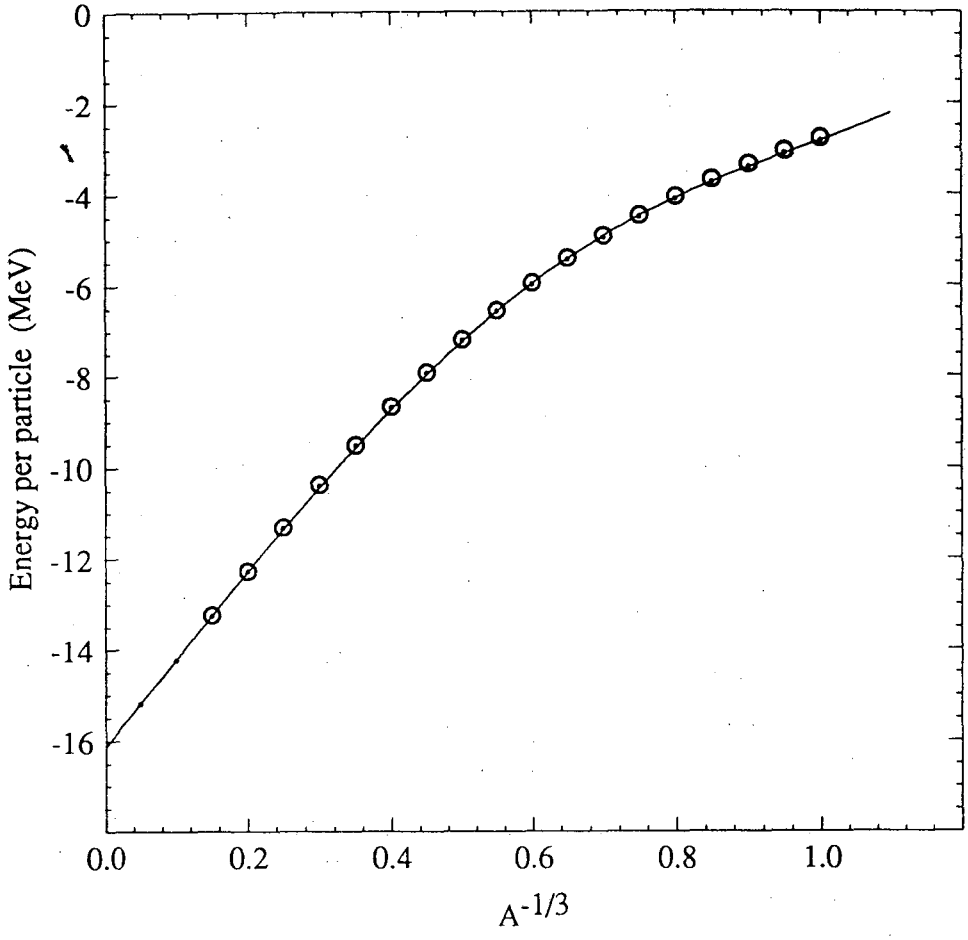

Figure 11: In this figure the solid dots correspond to the energy per particle calculated using a one dimensional, highly accurate numerical procedure for a sequence of spherical nuclei with $N = Z$ and no Coulomb energy, having particle numbers from 8000 down to 1. The circles represent the corresponding quantity calculated using the 3D lattice calculation. The solid line corresponds to a Droplet Model prediction supplemented by two adjusted higher order terms.

the nuclear energy and, in particular, the correctness of the Droplet Model form of the $A^{-2/3}$ term.

8 Acknowledgements

The authors wish to acknowledge discussions with J.R. Nix and A.J. Sierk and the substantial contributions that P. Möller made by determining the model parameters from a fit of the calculated binding energies to the measured masses of nuclei. We would like to thank E.W. Bethel for assistance with the computer-generated Figures 4 and 10.

References

[1] W. D. Myers and W. J. Swiatecki, Ann. Phys. (N. Y.) **204** (1990) 401-31.

[2] M. Brack, C. Guet and H.-B. Håkansson, Phys. Rep. **123** (1985) 275-364.

[3] A. K. Dutta, J.-P. Arcoragi, J. M. Pearson, R. Behrman and F. Tondeur, Nucl. Phys. **A458** (1986) 77-94.

[4] F. Tondeur, A. K. Dutta, J. M. Pearson and R. Behrman, Nucl. Phys. **A470** (1987) 93-106.

[5] J. M. Pearson, Y. Aboussir, A. K. Dutta, R. C. Nayak, M. Farine, and F. Tondeur, preprint (1990).

[6] B. Friedman and V.R. Pandharipande, Nucl. Phys. **A361** (1981) 502.

[7] P. Möller, private communication, November 1989.

[8] A. J. Sierk, private communication, April 1990.

[9] A. J. Sierk, Phys. Rev. **C33** (1986) 2039-53.

[10] G. Münzenberg, Rep. Prog. Phys. **51** (1988) 57, Fig. 17.

[11] W. D. Myers, "Droplet Model of Atomic Nuclei", IFI/Plenum, New York, 1977.

[12] P. Möller, J. R. Nix and W. J. Swiatecki, Nucl. Phys. **A492** (1989) 349.

[13] H. de Vries, C.W. Jager and C. de Vries, At. Data Nucl. Data Tables **36** (1987) 495-536.

[14] F. Garcias, M. Barranco, J. Nemeth and C. Ngô, Phys. Lett. **206B** (1988) 177.

[15] F. Garcias, M. Barranco, J. Nemeth, C. Ngô and X. Viñas, "Proc. of the Symposium on Nuclear Dynamics and Nuclear Disassembly", Dallas, Texas (1989).

[16] W. Stocker, J. Bartel, J. R. Nix and A. J. Sierk, Nucl. Phys. **A489** (1988) 252.

[17] P. Ring and P. Schuck, "Nuclear Many Body Problem",Springer-Verlag, 1980.

[18] H. J. Krappe, J. R. Nix and A. J. Sierk, Phys. Rev. **C20** (1979) 992.

[19] R. W. Hasse and W. D. Myers, "Geometrical Relationships of Macroscopic Nuclear Physics", Springer-Verlag, 1988.

[20] W. D. Myers and W. J. Swiatecki, Ann. Phys. (N. Y.) **55** (1969) 395.

LAWRENCE BERKELEY LABORATORY
UNIVERSITY OF CALIFORNIA
INFORMATION RESOURCES DEPARTMENT
BERKELEY, CALIFORNIA 94720